Princeton Plasma Physics Laboratory

PPPL- 4309

PPPL- 4309

Scrape-Off-Layer Current Model for Filament Structure Observed during Edge Localized Modes (ELMs) in DIII-D Tokamak

Hironori Takahash, E. D. Fredrickson, and M.J. Schaffer

April 2008

Prepared for the U.S. Department of Energy under Contract DE-AC02-76CH03073.

Princeton Plasma Physics Laboratory
Report Disclaimers

Full Legal Disclaimer

This report was prepared as an account of work sponsored by an agency of the United States Government. Neither the United States Government nor any agency thereof, nor any of their employees, nor any of their contractors, subcontractors or their employees, makes any warranty, express or implied, or assumes any legal liability or responsibility for the accuracy, completeness, or any third party's use or the results of such use of any information, apparatus, product, or process disclosed, or represents that its use would not infringe privately owned rights. Reference herein to any specific commercial product, process, or service by trade name, trademark, manufacturer, or otherwise, does not necessarily constitute or imply its endorsement, recommendation, or favoring by the United States Government or any agency thereof or its contractors or subcontractors. The views and opinions of authors expressed herein do not necessarily state or reflect those of the United States Government or any agency thereof.

Trademark Disclaimer

Reference herein to any specific commercial product, process, or service by trade name, trademark, manufacturer, or otherwise, does not necessarily constitute or imply its endorsement, recommendation, or favoring by the United States Government or any agency thereof or its contractors or subcontractors.

PPPL Report Availability

Princeton Plasma Physics Laboratory:

http://www.pppl.gov/techreports.cfm

Office of Scientific and Technical Information (OSTI):

http://www.osti.gov/bridge

Related Links:

U.S. Department of Energy

Office of Scientific and Technical Information

Fusion Links

Scrape-Off-Layer Current Model for Filament Structure Observed during Edge-Localized Modes in the DIII-D Tokamak

Hironori Takahashi,[1] E. D. Fredrickson,[1] and M. J. Schaffer[2]
[1]*Princeton Plasma Physics Laboratory, Princeton, New Jersey, USA*
[2]*General Atomics, San Diego, California, USA*
(Received 4 October 2007; published 19 May 2008)

The plasma in tokamaks often exhibits a relaxation oscillation called the edge-localized mode (ELM), which is generally attributed to MHD instability driven by strong gradients at the plasma boundary. It is shown here that field-aligned currents flowing just outside the boundary may also play a role in the ELM process. The poloidal perturbation magnetic field during ELMs in the DIII-D tokamak calculated from measured currents can reproduce prominent observed features, including a narrow magnetic structure at the outboard midplane similar to filaments observed earlier in DIII-D and NSTX.

DOI: 10.1103/PhysRevLett.100.205001 PACS numbers: 52.35.Py, 52.55.Fa, 52.55.Rk, 52.70.Ds

Edge-localized modes (ELMs) are the most critical issue to be resolved in tokamak fusion research. Recent intensive studies [1] of ELMs have focused on MHD instability just inside the plasma boundary. The present Letter considers a new element—current flowing in the scrape-off-layer (SOL) just outside the plasma boundary.

The plasma boundary is among the least understood regions in toroidal confinement devices, including tokamaks, and may harbor the potential to significantly affect their performance. ELMs are a cyclical process of gradual thermal buildup followed by MHD instability leading to abrupt thermal collapse at the plasma edge in high-confinement mode (H-mode) discharges in tokamaks. Temporally and spatially concentrated heat and particles transported into divertors during ELMs may unacceptably shorten the life of target tiles for an economically viable reactor.

Magnetic field perturbations observed during ELMs are generally assumed to originate from the MHD instability in the early phase and mostly from equilibrium changes in the later phase. But poloidal variations of observed fields reveal features that are difficult to attribute to these origins, and suggest that the electrical current in the SOL is perhaps an obvious source of field. Such currents were discovered [2] in the course of ELM studies flowing along open field lines terminating at divertor tiles. Among scrape-off-layer current (SOLC) driving mechanisms are the thermoelectric potential arising from unequal electron temperatures at the ends of an open fieldline and inductive coupling to MHD modes. The finding [3] that the SOLC begins to rise before the thermal collapse raised the question whether the SOLC may play a causal role in the ELM process, particularly in the light of the SOLC's close proximity to the plasma boundary, and if so, whether control of the SOLC may offer a means of controlling ELMs. The development of a model of the SOLC that can be used to calculate the field perturbations during ELMs, consistent both with SOLC measured at divertor tiles and with the field observed at magnetic probes, is a key in answering these questions. The SOLC is represented as a collection of filaments whose geometrical shape is prescribed by the underlying plasma equilibrium. SOLC-generated field is not constrained to a global eigenmode structure, and can reproduce field features that are difficult to explain in terms of MHD modes. The SOLC has been observed [4] during other MHD activity. The present work may be relevant for a wider scope of MHD activity than ELMs alone.

The poloidal field perturbation B_θ was measured by Mirnov coils [5] installed on the interior surface of the vacuum vessel. The SOLC was measured by tiles instrumented with resistive current sensors [4]. The field and SOLC were examined during Type-I ELMs in lower single null macroscopically stationary diverted H-mode discharges in DIII-D. For the example discharge shown in Fig. 1, the toroidal magnetic field was $|B_t| = 1.76$ T and the plasma current, $|I_p| = 1.34$ MA. Figure 1(a) schematically shows the SOLC flowing in successive "onion-skin" layers with alternating polarities. The layer immediately adjacent to the separatrix has been observed to carry current in the same toroidal direction as the Ohmic current ("forward" SOLC). The next layer carries current in an opposite toroidal direction ("backward" SOLC). An instrumented tile measures *net* current. The forward SOLC flows poloidally from the outboard to inboard divertor for the discharge studied here. Both forward and backward SOLCs circumnavigate the plasma poloidally. The outboard segment of a flux surface interrupted by parts of the limiter covering the top divertor baffle, such as the one designated as "3," may carry SOLC in either direction. Net SOLC through a single tile is compared in Fig. 1(b) with waveforms of B_θ and D_α light for an ELM. (SOLC and B_θ signals were smoothed to attenuate coherent oscillations at $\sim$22.4 kHz persisting over many ELMs.) The three signals, all from the inboard divertor region, had similar ELM onset time of $\sim$2722.7 ms and peak time of $\sim$2723.4 ms. The ELM process includes a fast-growing MHD mode accompanied by a thermal collapse, typically within the first few hundred μs. The modeling of B_θ discussed in this

 © 2008 The American Physical Society

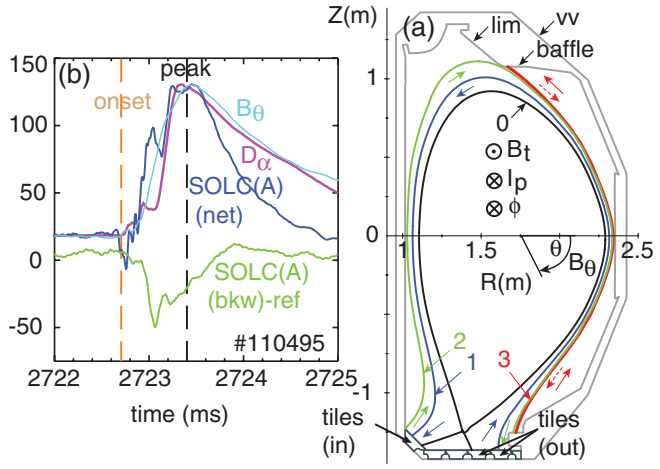

FIG. 1 (color). (a) Poloidal cross sections are shown of plasma separatrix (0), flux surfaces in the SOL (1, 2, and 3), vacuum vessel (vv) and limiter (lim) interior surfaces, and toroidal rings of tiles. Short arrows show poloidal directions of SOLC flow. φ and θ are toroidal and poloidal angles. (b) Net SOLC (forward minus backward) through a tile in units of amperes is shown during an ELM. (Backward SOLC, measured separately, is also shown.) Waveforms of B_θ and D_α light, both vertically shifted and scaled, are also plotted for comparison.

article pertains to the peak time, attained well after this initial fast transient stage.

Two qualitatively different building blocks for constructing the field are sketched in Fig. 2, circumnavigating and interrupted SOLC filaments. Both filaments sweep across the outboard midplane only once at high pitch angles, and could generate a narrow magnetic feature. A circumnavigating filament, making multiple toroidal turns on the inboard side at smaller pitch angles, generates field there with broader spatial scales. Unlike a fieldline in the plasma interior, which closes onto itself only on a rational surface, a SOLC filament on any flux surface can complete its closed circuit through tokamak structure.

B_θ was determined during the subject ELM by numerically integrating signals (dB/dt) from a set of 21 Mirnov

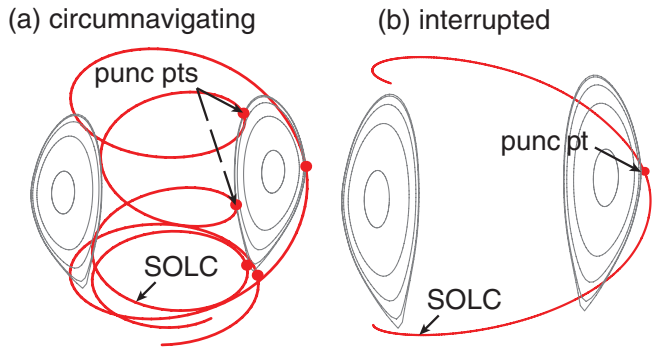

FIG. 2 (color). Two types of SOLC filaments—building blocks for field calculations—are shown: (a) poloidally circumnavigating and (b) interrupted trajectories. End points are on divertor tiles. SOLC circuits close through vessel wall. Flux surfaces and puncture points are visualization aids.

coils in a poloidal array at $\varphi = 38$ deg, and a set of 11 coils in a toroidal array at $\theta = 0$ deg (outboard midplane). Three of the signals are shown for each array in Fig. 3. The change in the field is examined from its value at the ELM onset time (left vertical dashed line). The perturbation field is assumed to return to zero by the next ELM onset (right vertical dashed line). The largest field measured by either array was from the bottom inboard divertor region [$\theta = +116$ deg in Fig. 3(a)], and reached a peak value of ~8.3 mT, ~0.7 ms after the ELM onset. The signal decayed from its peak with two disparate time scales, initially with an e-folding time of ~1.5 ms over ~2 ms, and then nearly linearly over ~10 ms toward the next ELM. The two signals shown in Fig. 3(b) ($\varphi = 48$ and 53 deg) were typical of the field at the outboard midplane. A third signal ($\varphi = 43$ deg) had an initial positive "jump," reaching a peak of ~1.8 mT in ~0.24 ms. Slower variation over the next 7 ms paralleled that of the other two signals. The contribution from the initial jump then decayed in the last 5 ms toward the next ELM. Observation of signals with an initial jump was sporadic; e.g., this signal behaved "normally" in the next ELM cycle [after ~2736 ms in Fig. 3(b)]. The 8 other signals of the toroidal array not shown in Fig. 3(b) were within range bars, ~0.8 mT.

The poloidal variation of B_θ, shown in Fig. 4(a), exhibits three idiosyncratic features: (i) it is largest in the bottom divertor, creating a "necklike" structure in the poloidal profile, (ii) larger on the inboard than outboard side ("anti-ballooning"), making a "headlike" feature, and (iii) small

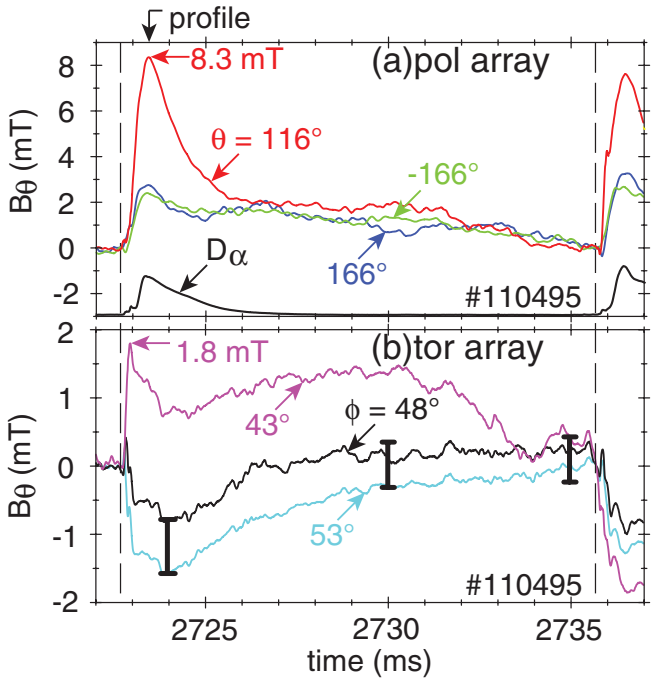

FIG. 3 (color). Evolution of B_θ from Mirnov coils in (a) poloidal array and (b) toroidal array. D_α light from the inboard divertor is also shown in (a). The arrow at the top indicates the time for field profile calculations.

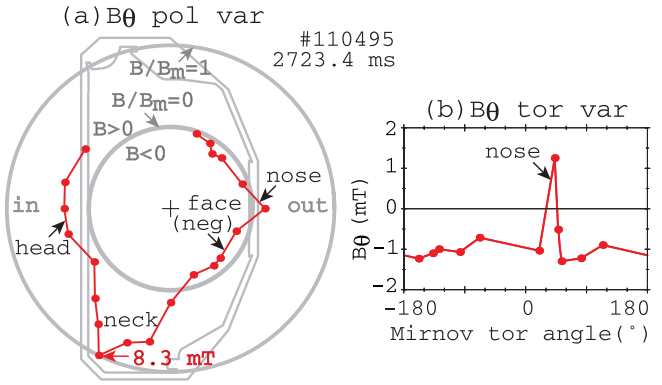

FIG. 4 (color). (a) Poloidal variation of measured B_θ at the ELM peak time presented in a modified polar plot: the field measured by a Mirnov coil ("dots") is proportional to length along a radial line drawn at the poloidal angular location of the coil as in a standard polar plot, but the length is measured from the inner circle ($B_\theta = 0$), toward the outer circle ($B_\theta = B_{\theta\,\mathrm{max}}$) for positive values and toward the origin ($B_\theta = -B_{\theta\,\mathrm{max}}$) for negative values. Overlaid are contours of the limiter and vacuum vessel for relating field variation to machine geometry. (No data were taken in the top region.) (b) Toroidal variation of B_θ at the peak time.

but mostly negative on the outboard ("face") side. These features were commonly observed in other ELMs. Additionally, a "noselike" structure was also observed in this ELM on the outboard side, a manifestation of the signal with a jump shown in Fig. 3(b). The nose was ~2.2 mT above its surrounding level, Fig. 4(b), at most 33 deg wide toroidally at its base, or at most ~8 deg wide poloidally after taking into consideration the fieldline pitch angle, ~15 deg, at the outboard midplane and postulating a field-aligned structure. The nose was nearly steady in amplitude and spatial location over a long period (~7 ms) in this ELM cycle. B_θ was negative, ~ -1 mT, at all measured locations, with a peak-to-peak variation of ~0.8 mT, except in the nose, suggesting that the negative face in the poloidal profile in Fig. 4(a) represented mostly an axisymmetric change.

The toroidal distribution of SOLC measured at the ELM peak time at 6 locations in the inboard divertor is shown in Fig. 5(a). Magenta dots represent the current density in units of A/deg (current flowing through a tile divided by the tile toroidal width, 7.5 deg). The radial SOLC profile at the ELM peak has been determined only on an event-averaged basis, without time resolution, by the "swept strike point" method (Ref. [4], Sec. 6). Figure 5(b) shows a SOLC radial profile (gray curve) as function of the flux surface separation (ΔR) from the separatrix at the midplane. The radial profile is bipolar: the positive lobe represents a toroidally and radially integrated poloidal current, $I_a \sim 9.2$ kA, and the negative lobe, $I_b \sim -3.5$ kA. SOLC measurement determines a total net current (~5.7 kA) integrated over the bipolar profile. Flux surfaces beyond $\Delta R \sim 4.5$ cm [gray vertical dashed line in Fig. 5(b)] are interrupted by the top divertor baffle. The SOLC-generated

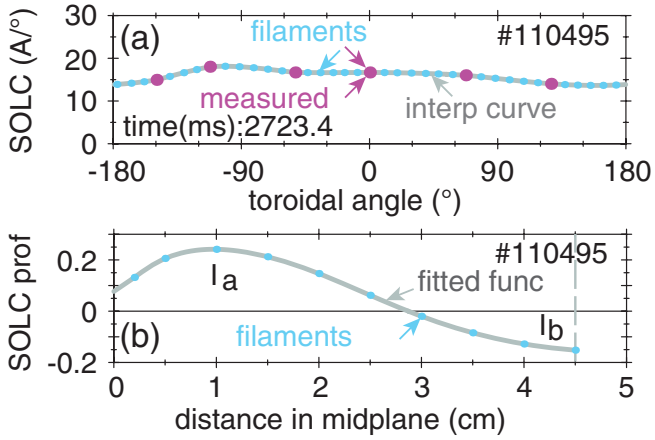

FIG. 5 (color). (a) Toroidal variation of SOLC density: measured values (magenta dots) in units of A/deg, interpolating curve (gray curve), and interpolation evaluation points (cyan dots). (b) Radial profile shape of SOLC density in relative units: event-averaged measured profile function (gray curve) and function evaluation points (cyan dots).

B_θ is calculated using a set of 10 radially distributed filaments following the magnetic field at each of 38 toroidal locations. The filaments are assigned a set of relative currents given in Fig. 5(b) to match the profile shape and the measured or interpolated current at that toroidal location, shown in Fig. 5(a). An additional backward current, $I_c = -16.5$ kA, was needed on the interrupted flux surface at $\Delta R = 5.7$ cm with a toroidal distribution given in Fig. 5(a) to reproduce the negative B_θ on the face. Further, the assumption of a single SOLC filament carrying forward current, $I_d = 0.8$ kA, on the interrupted flux surface at $\Delta R = 6$ cm was used to match the nose. (These interrupted flux surfaces are outside the coverage area of the outboard SOLC sensors.)

The model B_θ poloidal pattern in Fig. 6(a) reproduces well all three idiosyncratic features of the measured profile: the field peaks in the divertor (neck), larger on the inboard (head) than outboard side (antiballooning), and

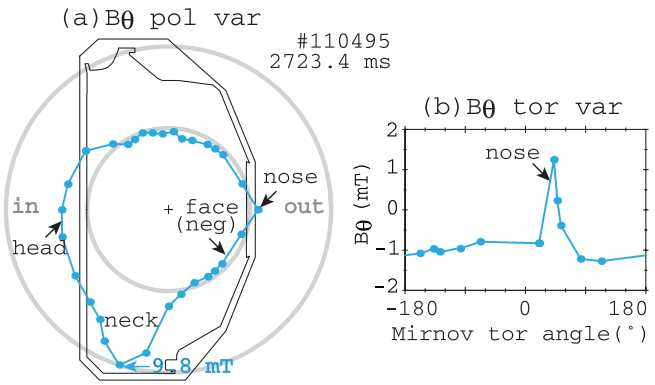

FIG. 6 (color). (a) Poloidal variation of calculated B_θ at the ELM peak time. See caption to Fig. 4 for presentation format. (b) Toroidal variation of calculated B_θ.

small and negative on the outboard side (face). It is the generic geometrical characteristics of the SOLC path, Fig. 2, that generate the idiosyncratic features, making their existence robust with respect to assumptions used in the calculation. The model B_θ toroidal variation in Fig. 6(b) quantitatively reproduces the measured one, including the height of the nose. Unusual field structures, such as the nose discussed in this Letter, are observed infrequently, but demonstrate that highly localized field does occur.

In conclusion, a model was developed for the SOLC represented as a collection of filaments whose geometrical shapes are prescribed by the underlying plasma equilibrium, and applied to calculations of field at Mirnov coil locations during the ELM. The calculated field at the ELM peak time reproduces prominent features of the measured one, both in poloidal and toroidal profiles. The observed SOLC is thus the likely source of the measured perturbation field at the peak of the ELM studied.

Discussion—The prominent features of the observed poloidal profile of the field, such as the neck and antiballooning characteristics, are significantly different from field patterns generally believed to exist during linear MHD modes. Thermal collapse is substantially complete typically in less than $\sim$100 μs from the ELM onset, and steep gradients at the plasma edge disappear well before the ELM peak time, $\sim$700 μs for the ELM examined here, making it unlikely that unusual features, like the nose described here, were a nonlinear manifestation (coalescence) of the MHD mode causing thermal collapse. It is not precluded, however, that the MHD mode played a role in the nose's formation. Part of the observed antiballooning feature may be produced by a radial plasma shift caused by thermal loss. The shift estimated [6] from the Shafranov equilibrium formula is, however, on the order of 0.1 mT at the ELM peak time, which is smaller by an order of magnitude than the observed value, $\sim$2.7 mT. Thus, the observed antiballooning feature was likely to be primarily due to a SOLC-generated field.

Evidence of current-carrying filaments during ELMs has been reported on DIII-D [7] and NSTX [8]. Two rotating helical filaments were observed [7] with the Mirnov diagnostic, suggesting current, over a period $\sim$170 μs during a Type-I ELM. A single helical filamentary striation was observed [8] in NSTX, lasting over a period 0.2–1 ms during Type-V ELMs through multiple diagnostics, including Mirnov coils and a framing camera. The simultaneous observations correlated a magnetically detected current-carrying filament and an optically seen striation. Multiple helical striations seen [9] in MAST during Type-I ELMs through a framing camera have been compared to solar eruptions. Multiple striations have also been seen [1] in DIII-D through a framing camera. Observations of both current-carrying filaments [7] and optical striations [1] in DIII-D have been suggested as evidence for filaments found [10] in simulations of a nonlinearly growing peeling-ballooning mode. Localized high-density bursts have also been reported [11] in DIII-D. Relationships between the SOLC and these filament structures and striations observed earlier are a subject for future investigation.

On the one hand, the field measured at Mirnov coil locations, both in amplitude and spatial pattern, is fundamental to analysis in MHD mode identification and feedback control, equilibrium reconstruction, and machine operation. A large SOLC-produced field could significantly affect the analysis. On the other hand, the effect of a nonaxisymmetric field produced by the SOLC on MHD stability and stochastic field generation depends on the field on the plasma boundary (and rational surfaces). The SOLC that flows a few cm away from the plasma edge creates a field there much greater than that at Mirnov coil locations, $\sim$12 cm away from the plasma edge in the outboard midplane in the present experiment.

A SOLC-generated field may affect MHD modes at the plasma boundary, but the SOLC circuit depends on transport processes in the SOL and divertors. The SOLC may thus connect MHD stability inside the separatrix to transport outside. This complex coupled system is the subject of nascent research: the SOLC may play a role in triggering ELMs [3,12] through internal positive feedback [12] between modes and currents, destabilize [13] the resistive wall mode, and exchange momentum [13] with the tearing mode, generate stochastic field, or cause 3D plasma surface distortion. Actively driven SOLC may offer a method of controlling ELMs and other MHD instability. The model developed here could provide a quantitative underpinning for SOLC-generated fields in these studies.

This work was supported by the U.S. Department of Energy under Contracts No. DE-AC02-76CH03073 and No. DE-AC03-99ER54463. The authors gratefully acknowledge helpful discussions with Dr. E. J. Strait.

[1] M. Fenstermacher *et al.*, Plasma Phys. Controlled Fusion **45**, 1597 (2003) and references therein.
[2] P. J. Harbour *et al.*, J. Nucl. Mater. **162**, 236 (1989).
[3] H. Takahashi *et al.*, *32nd EPS Conference on Controlled Fusion and Plasma Physics* (Tarragona, Spain, 2005).
[4] H. Takahashi *et al.*, Nucl. Fusion **44**, 1075 (2004) and references therein.
[5] E. J. Strait, Rev. Sci. Instrum. **77**, 023502 (2006).
[6] M. Okabayashi *et al.*, Nucl. Fusion **21**, 271 (1981).
[7] E. J. Strait *et al.*, Phys. Plasmas **4**, 1783 (1997).
[8] R. Maingi *et al.*, Phys. Plasmas **13**, 092510 (2006).
[9] A. Kirk *et al.*, Phys. Rev. Lett. **92**, 245002 (2004).
[10] P. B. Snyder *et al.*, Phys. Plasmas **12**, 056115 (2005).
[11] J. Boedo *et al.*, Phys. Plasmas **12**, 072516 (2005).
[12] L.-J. Zheng, H. Takahashi, and E. D. Fredrickson, Phys. Rev. Lett. **100**, 115001 (2008).
[13] R. Fitzpatrick, Phys. Plasmas **14**, 062505 (2007).

The Princeton Plasma Physics Laboratory is operated
by Princeton University under contract
with the U.S. Department of Energy.

Information Services
Princeton Plasma Physics Laboratory
P.O. Box 451
Princeton, NJ 08543

Phone: 609-243-2750
Fax: 609-243-2751
e-mail: pppl_info@pppl.gov
Internet Address: http://www.pppl.gov